Aeroelastic Studies of a Rectangular Wing with a Hole: Correlation of Theory and Experiment

Howard J. Conyers[*], **Earl H. Dowell**, **Kenneth C. Hall**
Department of Mechanical Engineering and Materials Science
Duke University
Durham, NC, USA
howard.conyers@duke.edu, dowell@ee.duke.edu, kenneth.c.hall@duke.edu

Abstract − *Two rectangular wing models with a hole have been designed and tested in the Duke University wind tunnel to better understand the effects of damage. A rectangular hole is used to simulate damage. The wing with a hole is modeled structurally as a thin elastic plate using the finite element method. The unsteady aerodynamics of the plate-like wing with a hole is modeled using the doublet lattice method. The aeroelastic equations of motion are derived using Lagrange's equation. The flutter boundary is found using the V-g method. The hole's location effects the wing's mass, stiffness, aerodynamics and therefore the aeroelastic behavior. Linear theoretical models were shown to be capable of predicting the critical flutter velocity and frequency as verified by wind tunnel tests.*

Keywords: flutter, damaged wings, finite element method, doublet lattice method, wind tunnel experiments

1 Introduction

Fighter aircraft are subject to attack by highly accurate missile defense systems when flying in enemy territory. Ballistic missiles can create through-hole type damage in the lifting surface. The aircraft may not be destroyed depending on the hole location and the size of the hole. However, the fluid-structure interaction will change the wing's aeroelastic behavior. As a result, the flutter velocity for which the undamaged plane was designed to fly will change.

Over the past 50 plus years the open literature is scarce on the aeroelastic impact of ballistic damage on modern aircraft. The first work in this area was performed by Biot and Arnold in 1950 [1] as reported by Dr. Ronald Stearman at the University of Texas-Austin [2]. Dr. Stearman performed extensive research on signal detection of ballistic damage between the 1970's and 1980's. In 2007, the crack-induced effects on the aeroelasticity of unswept composite wings were investigated [3]. Otherwise, the research related to ballistic damage in the unclassified literature has focused on investigating the aerodynamics experimentally. In 1982, NASA published experimental findings on the aerodynamic effect of hole location caused by ballistic damage during certain flight conditions [4]. Other investigations include evaluating the effect of ballistic damage on the aerodynamics of helicopter rotor airfoils [5] and the effect of the shape of the hole used to simulate damage [6].

Aeroelastic studies on undamaged aircraft and wind tunnel models are found more frequently in the literature. Flutter and limit cycle oscillations have been studied experimentally and theoretically on various editions of the actual F-16 aircraft during flight tests for different external store (i.e., missiles and fuel tanks) configurations by Denegri and colleagues [7–10]. In order to improve the design methods for the F-16, wind tunnel models were designed using various theoretical models by Dowell, Tang, Attar [11–15] and Gordnier [16] to better understand the mechanisms causing flutter and limit cycle oscillations.

In the present study, a rectangular wing model with a hole has been designed where the hole simulates damage. The wing is modeled as a thin, uniform, elastic plate using the finite element method. The aerodynamic loads are computed using the linear frequency domain doublet lattice aerodynamic model [17–19]. The aeroelastic model is derived by coupling the aerodynamic and structural models using Lagrange's equation.

In this paper, two rectangular models with a hole are designed. The hole location varied in the spanwise location. The theoretical flutter velocity and frequency were validated against tests conducted at Duke University's subsonic wind tunnel.

2 Finite Element Method

The wing is modeled as a thin, elastic, and isotropic plate. These assumptions are categorized as the small deflection theory of bending because the "plane sections

[*]NASA Stennis Space Center

initially normal to midsurface remain plane and normal to that surface after bending [20]."

The finite element method uses the principle of virtual work to derive the structural model. The principle states that the change of strain energy due to the virtual displacement is equal to the change in external work due to applied forces, $\delta U = \delta W$. The Rayleigh Ritz Method is used with the principle of virtual work in the commercial finite element software, ANSYS$^{\text{TM}}$, to formulate the general equations of motion for the plate-like system.

$$\delta U = \int \{\delta\epsilon\}^T \{\sigma\}\, dV \tag{1}$$

$$\begin{aligned} \delta W &= \int (\{\delta u\}^T \{F\} + \{\delta u\}^T \rho \{\ddot{u}\}) dV \\ &\quad + \int \{\delta u\}^T \{\Phi\}\, dS \end{aligned} \tag{2}$$

$$\{u\} = [N]\{d\}, \{\ddot{u}\} = [N]\left\{\ddot{d}\right\} \tag{3}$$

Equations 1, 3, and 3 represent the principle of virtual work on the element level used in the finite element method where δ is the virtual operator, U is the strain energy, W is the external work, $\{u\}$ is the displacement vector, $\{F\}$ is the body forces vector, Φ is the matrix of surface tractions, and ρ is the density. The displacement vector ($\{u\}$) is composed of nodal displacements (d) and shape functions (N). The nodal displacements are the temporally dependent nodal degrees of freedom and the shape functions are spatially dependent. The shape functions in ANSYS$^{\text{TM}}$ vary with the type of element model used. Element SHELL63, a 4-node quadrilateral shell, is used here to model the uniform plate [21]. SHELL63 exhibits six degrees of freedom since it can translate and rotate in the x, y, and z directions and axes, respectively. The plate is clamped along the root. The cantilevered boundary condition is enforced by stating that no displacement and rotation occurs where the plate is clamped.

The generalized matrix form of the equations in Eqn. 4 is formulated by ANSYS$^{\text{TM}}$ after substituting the shape functions and the assumptions into Eqns. 1-3. In determining the natural frequencies and modes, the external loads (r^{ext}) in Eqn. 4 are assumed to equal zero. The resulting equation is solved in ANSYS$^{\text{TM}}$ by further assuming simple harmonic motion to remove the temporal dependence. The result is the classical eigenvalue problem that is solved using the Block Lanczos Method [21].

$$[m]\left\{\ddot{d}\right\} + [k]\{d\} = \left\{r^{ext}\right\} \tag{4}$$

2.1 Correlation of experiment with results from the finite element method

Consider Takahashi's experiment in the 1960's as reported by Leissa [22]. Takahashi examined a clamped steel rectangular plate on all edges with a centralized hole, see Fig. 1. The analysis and experiment varies the hole radius, R, for a range of R/a where a=0.2032 m. The nondimensional frequency predicted by ANSYS$^{\text{TM}}$ is lower than those found analytically by Takahashi, see Fig. 1. ANSYS$^{\text{TM}}$ is a higher fidelity structural model than the one used by Takahashi. Takahashi's model used products of beam modes.

3 Doublet Lattice Aerodynamic Method

The aerodynamics for the rectangular wing with a hole is modeled by potential flow theory. See the aerodynamic potential equation in Eqn. 5 where ϕ is the velocity potential, a_∞ is the speed of sound, and U_∞ is the free stream velocity. The far field boundary condition needed to solve Eqn. 5 states that the wave disturbances created by the lifting surface's motion propagate toward infinity with no reflections. As a result, all the wind tunnel walls are assumed to be infinitely far away accept for the tunnel's floor. The floor is accounted for by using the method of images. The other boundary condition, see Eqn. 6, states the normal velocity of the fluid at the surface equals the normal velocity of the body. For the thin wing in this work, $F(x,y,z,t) = z - f(x,y,t)$ in Eqn. 6 where $z = 0$ at the surface of the airfoil and $f(x,y,t)$ refers to the height of the wing surface above the plane.

$$\nabla^2\phi - \frac{1}{a_\infty^2}\left[\frac{\partial^2\phi}{\partial t^2} + 2U_\infty\frac{\partial^2\phi}{\partial x \partial t} + U_\infty^2\frac{\partial^2\phi}{\partial x^2}\right] = 0 \tag{5}$$

$$\frac{\partial F}{\partial t} + \vec{q}\cdot\nabla\vec{F} = 0 \tag{6}$$

The aerodynamic potential equation is transformed to a Kernel (integral) equation by using Green's Theorem. The Kernel (K) equation is solved numerically in Eqn. 7 using a distributions of doublets to relate pressure ($\bar{p}$) to downwash ($\bar{w}$) and the doublet lattice method [17]. Equation 7 is rewritten in matrix form in Eqn. 8 where D_{ij} is the kernal approximated using the doublet lattice method. The doublet lattice method is a "finite element approach" to approximate the kernel. The doublet lattice method divides the wing into a series of panels (boxes). One set of sides on the panels must be parallel to the freestream velocity.

$$\overline{w}(x,y) = \frac{1}{8\pi}\int_s\int K(x,\xi;y,\eta;\omega,M)\overline{p}(\xi,\eta)\mathrm{d}\xi\mathrm{d}\eta \tag{7}$$

$$\overline{w}_j = \sum_{j=1}^{n} D_{ij}\overline{p}_j \tag{8}$$

The doublet lattice method (DLM) is suitable to model the pressure across a planar wing with a hole. The DLM

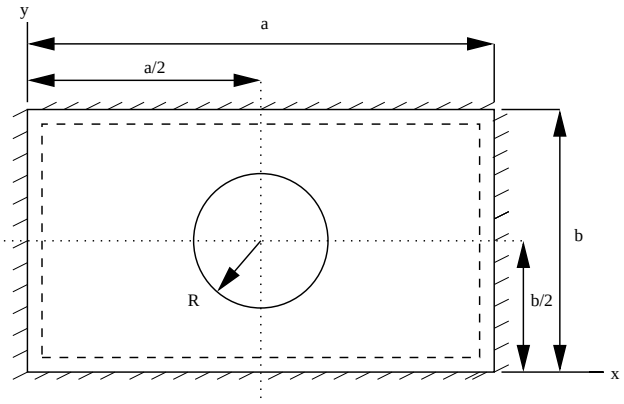

(a) Clamped rectangular plate having a centralized circular hole studied by Takahashi

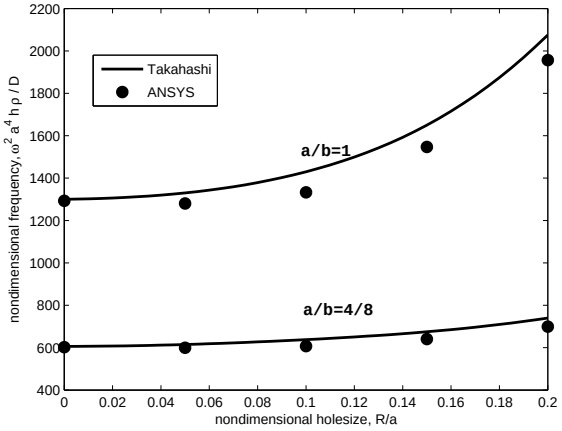

(b) Results for Takahashi and ANSYS$^{\text{TM}}$ for a/b=1/2 and a/b=1

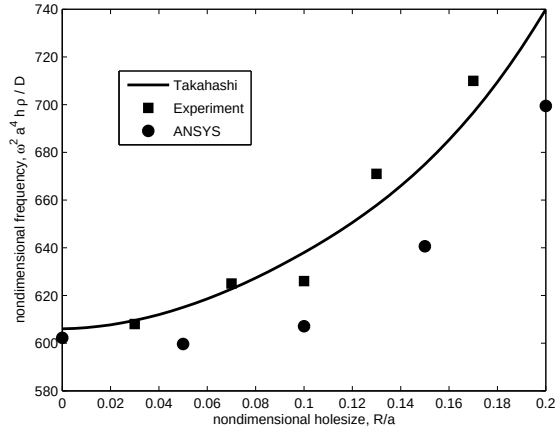

(c) Results from Takahashi, ANSYS$^{\text{TM}}$ and Experiment a/b=1/2, $\nu = 0.3$

Figure 1: Takahashi's experiment and a comparison using ANSYS. Plots of nondimensional frequency parameter $\frac{\omega^2 a^4 \rho}{D}$ as a function of hole size for a clamped rectangular plate. $D = Eh^3/12(1-\nu^2)$ is flexural rigidity.

methodology devised by Rodden and et al was used to calculate the aerodynamic influence coefficient matrix in a doublet lattice code written in-house [17, 19]. The in-house code does not use the substitution originally suggested by Rodden in that the steady portion calculated using the doublet lattice method should be replaced with the steady portion from the vortex lattice method. In addition, the code uses the quartic approximation used to improve the DLM [19]. The two unknowns in this problem are the pressure jump on the wing area around the hole and the downwash on the hole area. However, the latter is not needed in this work. In the hole region, the pressure jump equals to zero. The downwash on the wing portion around the hole is known. In determining the pressure over the portion of the wing surrounding the hole, all that is needed is to set the pressure to zero in the hole. The downwash and aerodynamic influence coefficient matrix are known, so its takes a simple matrix inversion to determine the unknown pressures.

The local doublet strength is proportional to the pressure jump, so in the wake and the hole, the doublet strength is zero. The wing aerodynamics with a hole requires setting the doublets' equation in the hole equal to zero. Computationally, it is easier to set $\bar{p} = 0$ since it is the same as not having any elements there at all. Initially, the aerodynamic influence coefficient matrix (AICM) is computed for a wing without a hole using the doublet lattice method. The panels where the holes are located affects the AICM and the downwash. The hole on the i^{th} panel is represented by having zeros on the i^{th} row of the AICM except for on the diagonal. At the diagonal location a one is placed on the i^{th} row. In the downwash vector a zero is placed on the i^{th} row to force $\bar{p} = 0$, see Eqn. 9. The substitutions are repeated for every panel on the wing that the hole region covers.

$$\begin{Bmatrix} w_1 \\ 0 \\ \vdots \\ w_n \end{Bmatrix} = \begin{bmatrix} D_{11} & D_{12} & \cdots & D_{1n} \\ 0 & 1 & 0 & 0 \\ \cdots & \cdots & \cdots & \cdots \\ \vdots & \vdots & \vdots & \vdots \\ D_{n1} & & \cdots & D_{nn} \end{bmatrix} \begin{Bmatrix} p_1 \\ p_2 \\ \vdots \\ p_n \end{Bmatrix} \quad (9)$$

4 Aeroelastic Analysis

The aeroelastic model couples the structural and the aerodynamic models. The aeroelastic equations are formulated using Lagrange's equations and modal methods. The only caveat is the structural and aerodynamic grids are different.

$$\frac{d}{dt}\frac{\partial L}{\partial \dot{q}_i} - \frac{\partial L}{\partial q_i} = Q_i \quad (10)$$

The two unknowns in Lagrange's equation, see Eqn. 10, are the Lagrangian (L) and the generalized forces (Q_i). The Lagrangian is the difference between the kinetic and potential energy of a structure. The generalized forces

are computed from the aerodynamic forces. The Lagrangian is computed using the natural modes and frequencies obtained from the structural theory. The first 10 out of 1000 natural modes found in ANSYS^{TM} are retained for the aeroelastic model. Generally, the lowest modes have the greatest impact on aeroelastic behavior. The natural modes and frequencies are used in a modal series expansion. The modal series expansion, Eqn. 11, contains the generalized coordinate ($q_m(t)$) and the natural mode ($z_m(x,t)$).

$$z_a = \sum_m q_m(t) z_m(x,y) \tag{11}$$

The kinetic and potential energy expressions in Eqn. 12 and Eqn. 13, respectively requires knowing the generalized mass (M_m) and stiffness (K_m). The generalized mass is computed from Eqn. 14 where m_a is the mass per unit area. The use of natural modes reduces the computation of the stiffness matrix to the mass matrix times the natural frequencies.

$$T = 1/2 \sum_m M_m \dot{q}_m^2 \tag{12}$$

$$V = 1/2 \sum_m K_m q_m^2 \tag{13}$$

$$M_m \equiv \int\int m_a z_m^2 dxdy \tag{14}$$

The generalized aerodynamic forces are computed from the pressures found using the doublet lattice method. The downwash in Eqn. 15 is needed by the DLM and it comes from the natural mode deflection and the slope of deflection. As is, the deflection points of the natural mode do not match the aerodynamic grid, so a polynomial curve-fitting technique is applied using a least squares method. A fifth order polynomial is fitted to each natural mode to determine the polynomial coefficients needed to characterize the mode. The mode characterization allows the deflections to be found at any x and y, which is used in calculating the downwash for DLM.

$$\frac{w}{U} = \frac{1}{U}\frac{\partial z_a(x,y,t)}{\partial t} + \frac{\partial z_a(x,y,t)}{\partial x}. \tag{15}$$

The natural modes simplifies computing the mass and stiffness matrices for the aeroelastic model to just the terms along the diagonal. The polynomial's accuracy is evaluated by looking at the diagonal terms in the mass matrix since it should approximately equal one when normalized. The generalized forces are computed from the downwash found using the polynomial in the doublet lattice method. Using Eqns. 11-14, Lagrange's equation condenses to Eqn. 16. The aerodynamic loads are computed as a function of nondimensional frequency (k) in the summation $\sum_m A_{mi}(k) q_m$.

$$\sum_m M_{mi}\ddot{q_m} + K_{mi} q_m = \frac{\rho U^2}{2} \sum_m A_{mi}(k) q_m \equiv Q_i \tag{16}$$

The nondimensional frequency k that is needed to compute the aerodynamics is well suited for the V-g method in the aeroelastic analysis. The V-g method multiplies the stiffness matrix by $1 + ig$ where g is the fictitious damping adding to find the neutrally stable solutions. Additionally, simple harmonic motion ($q = \bar{q}^{i\omega t}$) is assumed so $\bar{q}$ can be factored out of Eqn. 16. Equation 16 is rearranged for the V-g method, see Eqn. 17. At each iteration of k, ω^2 and g are calculated. Recalling $k = \omega b/U$, therefore the velocity (U) can be computed since k is prescribed, ω is calculated, and the semichord b is known. The specific velocity where flutter occurs corresponds to $g = 0$. When g equals zero the original aeroelastic equation (Eqn. 16) is recovered.

$$\left\{ -[M] + \frac{1+ig}{\omega^2}[K] - \frac{\rho b^2}{2k^2}[A(k)] \right\} \{\bar{q}\} = 0 \tag{17}$$

5 Results

The two designed aeroelastic cantilever rectangular wings are made of polycarbonate with a thickness of 0.001588 m, a chord of 0.1524 m (6 in), and a length of 0.3048 m (12 in). The plate's material properties are the followimg: ρ=1217 kg/m^3, E= 2.4e9 N/m^2, and ν= 0.33. In Model A, see Fig. 2, the rectangular hole measures with a = 0.057 m (2.25 in) and b =0.095 m (3.75 in). The base of the hole is 0.0579 m from the root chord and 0.048 m from the leading edge. The hole size and the amount of mass removed is roughly 12% of the total wing. Model B is identical to Model A except the hole location goes outward in the spanwise location. The base of the hole in Model B is 0.1524 m from the root chord and 0.048 m from the leading edge. The struc-

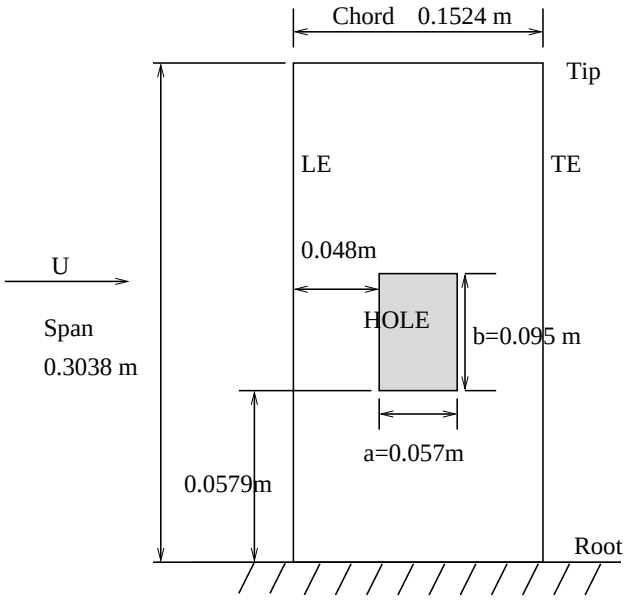

Figure 2: Dimensional drawing of rectangular wing with a rectangular hole near root

Table 1: Comparison of theory (The.) and experiment (Exp.) for first five natural frequencies (in Hz) for cantilivered rectangular wing with rectangular hole near the root and tip. Bend. and Tors. refer to the bending and torsion mode, respectively

		No Hole		Model A		Model B	
mode no.	mode char.	The.	Exp	The.	Exp.	The.	Exp.
1	Bend.	3.99 Hz	4.13 Hz	3.49 Hz	3.50 Hz	4.20 Hz	4.25 Hz
2	Tors.	16.95	17.25	15.08	15.50	16.02	16.13
3	Bend.	24.86	24.38	24.69	25.00	23.24	23.75
4	Tors.	55.33	54.25	53.28	53.75	50.10	51.25
5	Bend./Tors.	69.84	69.00	71.99	73.65	66.25	68.00

tural behavior for the rectangular plates was found theoretically using the finite element method in ANSYS^{TM}. The structural behavior was tested experimentally using a vibration test for the first five natural frequencies, see Table 1. The lower frequencies are known to have the largest impact on aeroelastic behavior. The structure was excited using a Brüel & Kjaer (B&K) 4810 mini-shaker mounted with a B&K 8200 force transducer. The structure's response was recorded using the B&K type 4375 accelerometer placed farthest away from the shaker near the tip of the cantilevered plate. The shaker is powered by an external power amplifier that is provided a pseudo random signal from the B&K 4 Channel PULSE^{TM} 3560-T-C, the front-end data acquisition system. PULSE^{TM} is an advanced software/hardware analyzer platform developed by Brüel & Kjaer for data acquisition and analysis. PULSE^{TM} determines the frequency response by performing a fast fourier transform analysis of the acceleration time series data.

The correlation between theory and experiment for the structural analysis is good. The theoretical structural models require about 1000 finite elements to achieve convergence. The results are observed to behave according to beam theory even though a plate is modeled. The natural frequencies decrease in Model A when the hole is closer to the root. This suggests that "stiffness effects" are more dominant than mass effects in this region. The natural frequencies increase in Model B when the hole is closer to the tip. This suggests that "mass effects" are more dominant in this region.

The aeroelastic model was developed using the method outlined in the previous section. The doublet lattice method included 256 panels across the wing (512 total for mirror image) with 16 divisions in the chordwise direction and 16 divisions in the spanwise direction to calculate the generalized forces. The hole consumes 30 panels.

The flutter frequency was determined experimentally using the PULSE^{TM} data acquisition system with an accelerometer fixed near the root chord on the trailing edge. The velocity of the windtunnel at flutter was read from a voltmeter connected to a pitot static tube. The experimental flutter velocity and frequency are generally in good agreement with the theory, see Table 2.

Table 2: Theoretical and experimental flutter velocity and frequency listed for cantilevered rectangular wing with rectangular hole

	No Hole		Model A		Model B	
	The.	Exp.	The.	Exp.	The.	Exp.
U_f in m/s	20.8	20.05	21.5	20.65	25.3	25.2
ω_f in Hz	10.3	11.50	8.5	9.18	8.3	9.4

6 Conclusions

Flutter of a rectangular cantilever wing was predicted using the finite element method and the doublet lattice method in forming the aeroelastic model with Lagrange's equation. The flutter velocities and frequencies are reported for a rectangular wing without a hole and for a rectangular wing with a hole in two different spanwise locations. Linear models are incapable of determining the flutter amplitude.

The agreement between theory and experiment for flutter is generally good for a hole that is 12% of the wing area for configurations analyzed. The interesting behavior is the increase in the flutter velocity from the case without a hole. One might anticipate the flutter velocity would decrease due to the presence of a hole, but the theory and experiment indicate the opposite. Further, calculations for other sizes showed expected results. For a model with a hole size of 6% the effect of flutter is small.

Developing a model for a hole size of 6% of the wing area yields changes that do not make a noticeable impact in investigating the stuctural behavior and the aerodynamics independently. Quite the opposite, a hole area 25% of the wing makes a large impact but the structure is challenged from its own inertia loads before even considering the aerodynamics loads.

Future work may evaluate using a time marching code to model the aerodynamics of a wing with a hole to develop nonlinear aeroelastic models. To date there is no time marching code that is capable of modeling aerodynamics of a wing with a hole. However, a clever substitution similar to the one implemented for the doublet lattice code could be potentially derived.

Acknowledgment

The authors would like to thank Ronald Stearman of the University of Texas-Austin, Max Blair of Wright-Patterson Air Force Base, Peter Attar of the University of Oklahoma, and William Rodden for their insights and support of this work.

References

[1] M.A. Biot and L. Arnold, *Study of vulnerability of aircraft to damage induced flutter*, Ballistic Research Laboratories, 743, Oct. 1950.

[2] G. Chen and R.O. Stearman, "A damage induced aeroelastic failure mode involving combination and parametric resonant instabilities of lifting surfaces," in *A Collection of Technical Papers Part 2: Structural Dynamics and Design Engineering*, AIAA/ASME/ASCE/AHS 23rd Structures, Structural Dynamics and Material Conference, May 1982.

[3] K.H. Wang and D.J. Inman, "Crack-induced effects on aeroelasticity of an unswept composite wing," *AIAA journal*, Vol. 45, No. 3, pp. 542–551, 2007.

[4] M.L. Stearman, *Wind-tunnel studies of the effects of simulated damage on the aerodynamics characteristics of airplanes and missiles*, NASA Technical Manual (TM)-84588, Dec. 1982.

[5] K.W. Robinson and J.G. Leishman, "Effects of ballistic damage on the aerodynamics of helicopter rotor airfoils," *Journal of aircraft*, Vol. 35, No. 5, pp. 695–703, 1998.

[6] P.M. Render, S. De Silva, A. Walton and M. Mani, "Experimental investigation into the aerodynamics of battle damaged airfoils," *Journal of aircraft*, Vol. 44, No. 2, pp. 539–549, 2007.

[7] C.M. Denegri Jr., "Limit cycle oscillation flight test results of a fighter with external stores," *Journal of aircraft*, Vol. 37, No. 5, pp. 761–769, Sep.–Oct. 2000.

[8] R.W. Bunton and C.M. Denegri Jr., "Limit cycle oscillation characteristics of fighter aircraft," *Journal of aircraft*, Vol. 37, No, 5, pp. 916–918, Sep.–Oct. 2000.

[9] C.M. Denegri Jr. and M.R. Johnson, "Limit cycle oscillation prediction using arti

cial neural networks," *Journal of guidance, control, and dynamics*, Vol. 24, No. 5, pp. 887–895, Sep.–Oct. 2001.

[10] C.M. Denegri Jr., J.A. Dubben and D.L. Maxwell, "In-flight wing deformation characteristics during limit-cycle oscillations," *Journal of aircraft*, Vol. 42, No. 2, p. 500–508, Mar.–Apr. 2005.

[11] P.J. Attar, E.H. Dowell and J.R. White, "Modeling the LCO of a delta wing using a high fidelity structural model," *Journal of aircraft*, Vol. 45, No. 2, pp. 1209–1217, Sep.–Oct. 2005.

[12] D.M. Tang, J.K. Henry and E.H. Dowell, "Limit-cycle oscillations of delta wing models in low subsonic flow," *AIAA journal*, Vol. 37, No. 11, pp. 1355–1362, Nov. 1999.

[13] D.M. Tang, P.J. Attar and E.H. Dowell, "Flutter/LCO analysis and experiment for wing-store model, *AIAA journal*, Vol. 44, No. 7, pp. 1662–1675, 2006.

[14] D.M. Tang and E.H. Dowell, "Flutter and limit cycle oscillations for a wing-store model with freeplay," *Journal of aircraft*, Vol. 43, pp. 487–603, Mar.–Apr. 2006.

[15] D.M. Tang and E.H. Dowell, "Experimental/theoretical correlation study of gust response for a wing-store model with freeplay," *Journal of sound and vibration*, Vol. 295 Nos. 3-5, pp. 659–684, 2006.

[16] R.E. Gordnier, "Computation of limit-cycle oscillations of a delta wing," *Journal of aircraft*, Vol. 40, pp. 1206–1208, Nov.-Dec. 2003.

[17] E. Albano and W.P. Rodden. "A doublet-lattice method for calculating lift distributions on oscillating surfaces in subsonic flows," *AIAA journal*, Vol. 7, No. 2, pp. 279–284, Feb. 1969.

[18] W.P. Rodden, J.P. Giesing and T.P. Kalman, "Refinement of the nonplanar aspects of the subsonic doublet-lattice lifting surface method," *Journal of aircraft*, Vol. 9, No. 1, pp. 69–73, Jan. 1972.

[19] W.P. Rodden, P.F. Taylor and S.C. McIntosh Jr, "Further refinement of the subsonic doublet-lattice method," *Journal of aircraft*, Vol. 35, No. 5, pp. 720–727, Sep.–Oct. 1998.

[20] A.C. Ugural, *Stresses in plates and shell*, McGraw Hill Companies, Inc., Boston, second edition, 1999.

[21] Swanson Analysis Systems Inc., *ANSYS user manual*, release 6.1, 2002.

[22] A.W. Leissa, *Vibration of plates*, NASA Technical Report, SP-160, 1969.